

This discussion paper is/has been under review for the journal Hydrology and Earth System Sciences (HESS). Please refer to the corresponding final paper in HESS if available.

# Estimate soil moisture using trapezoidal relationship between remotely sensed land surface temperature and vegetation index

W. Wang, D. Huang, X.-G. Wang, Y.-R. Liu, and F. Zhou

State Key Laboratory of Hydrology-Water Resources and Hydraulic Engineering,  
Hohai University, Nanjing, 210098, China

Received: 26 October 2010 – Accepted: 26 October 2010 – Published: 3 November 2010

Correspondence to: W. Wang (w.wang@126.com)

Published by Copernicus Publications on behalf of the European Geosciences Union.

8703

## Abstract

The trapezoidal relationship between surface temperature ( $T_s$ ) and vegetation index (VI) was used to estimate soil moisture in the present study. An iterative algorithm is proposed to estimate the vertices of the  $T_s \sim VI$  trapezoid theoretically for each grid, and then WDI is calculated for each grid using MODIS remotely sensed measurements of surface temperature and enhanced vegetation index (EVI). The capability of using WDI based on  $T_s \sim VI$  trapezoid to estimate soil moisture is evaluated using soil moisture observations and antecedent precipitation in the Walnut Gulch Experimental Watershed (WGEW) in Arizona, USA. The result shows that,  $T_s \sim VI$  trapezoid based WDI can well capture temporal variation in surface soil moisture, but the capability of detecting spatial variation is poor for such a semi-arid region as WGEW.

## 1 Introduction

In 1980s', it was found that, land surface temperature ( $T_s$ ) and the fraction of vegetation cover, which is represented by vegetation indices (e.g., NDVI), typically show a strong negative relationship (e.g., Goward et al., 1985; Nemani and Running, 1989). Such a relationship has been widely used to investigate the moisture condition of land surfaces. Several studies focused on the slope of the  $T_s/NDVI$  curve for providing information on vegetation and moisture conditions at the surface (e.g., Smith and Choudhury, 1991; Nemani et al., 1993). Their approach was later extended to use the information in the  $T_s/VI$  scatter-plot space, whose envelope is considered to be in either a triangular shape (e.g., Price, 1990; Carlson et al., 1994), or a trapezoid shape (e.g., Moran et al., 1994).

The idea of triangle  $T_s/VI$  space has been used to develop the so called “triangle method”, and has been applied by a lot of researchers (e.g., Gillies et al., 1997; Sandholt et al., 2002; Margulis et al., 2005; Tang et al., 2010). The “triangle” method fits the scatter-plot of observed vegetation index (VI) and land surface temperature ( $T_s$ ) using

8704

a triangle. The central assumption of the triangle method is that, given a large number of pixels reflecting a full range of soil surface wetness and fractional vegetation cover, sharp boundaries (edges) in the data reflect real physical limits: i.e., bare soil, 100% vegetation cover, and lower and upper limits of the surface soil water content, e.g., completely dry or wet (field capacity), respectively. The dry and wet edges ultimately intersect at a (truncated) point at full vegetation cover. Then, based on the triangle, the relative value of surface soil water content and the surface energy fluxes at each pixel can be defined in terms of its position within the triangle. The advantage of the triangle method is its independence of ancillary data. The approach, however, has difficulty in defining the dry and wet edge, especially the dry edge. Even with a large number of remotely sensed observations, the boundaries of the triangle space are still hard to be well established, because on one hand, there are situations when  $VI-T_s$  points scatter in a close range such as during rainy season or in areas with a narrow VI range; on the other hand, the  $T_s \sim VI$  relationship is much more complicated at large scale than at local scale and may vary at different parts due to heterogeneity in land surface properties and atmospheric forcing. Furthermore, because the triangle space is established empirically, the soil moisture estimates according to such an empirical triangle using an image at one time are hard to be compared with those at another time.

Moran et al. (1994) proposed the idea of vegetation index/temperature (VIT) trapezoid, and the water deficit index (WDI) for evaluating evapotranspiration rates of both full-cover and partially vegetated sites. However, very few applications were found in the literature based on the idea of trapezoid  $T_s/VI$  space for estimating soil moisture. In the present paper, we will extend the idea of VIT trapezoid and WDI, for estimating soil moisture estimation using MODIS products. The method, referred to as the trapezoid method, will be described in detail in Sect. 2. Then the method will be applied to the Walnut Gulch Experimental Watershed in Arizona, USA, for which, the data used and data pre-process will be introduced in Sects. 3 and 4, and the results will be presented in Sect. 5. Finally, some conclusions will be drawn in Sect. 6.

8705

## 2 Trapezoid method

### 2.1 The concept of $(T_s - T_a) \sim V_c$ trapezoid

Idso et al. (1981) and Jackson et al. (1981) proposed the CWSI (Crop Water Stress Index) for detecting plant water stress based on the difference between canopy and air temperature. It is designed for full-cover vegetated areas and bare soils at local and regional scales. To overcome the difficulty of measuring foliage temperature in partially vegetated fields, Moran et al. (1994) proposed to use the shape of trapezoid to depict the relationship between the surface temperature and air temperature difference ( $T_s - T_a$ ) vs. the fractional vegetation cover ( $V_c$ , ranging from 0 for bare soil to 1 for full-cover vegetation) (Fig. 1), so as to combine spectral vegetation indices with composite surface temperature measurements to allow application of the CWSI theory to partially vegetated fields without a priori knowledge of the percent vegetation cover. Based on the trapezoid assumption and the CWSI theory, Moran et al. (1994) introduced the Water Deficit Index (WDI) for evaluating field evapotranspiration rates and relative field water deficit for both full-cover and partially vegetated sites. For a given pixel with measured surface temperature and air temperature difference, i.e.,  $(T_s - T_a)_r$ , WDI is defined as:

$$WDI = \frac{(T_s - T_a)_{\min} - (T_s - T_a)_r}{(T_s - T_a)_{\min} - (T_s - T_a)_{\max}} \quad (1)$$

where  $T_a$  is air temperature;  $T_s$  is surface temperature; the subscripts min, max, and r refer to minimum, maximum, and measured values, respectively; and the minimum and maximum values of  $(T_s - T_a)$  are interpolated linearly on the cold edge and warm edge of the  $(T_s - T_a) \sim V_c$  trapezoid for the specific  $V_c$  value of the pixel. Graphically, WDI is equal to the ratio of distances AC/AB in Fig. 1.

8706

## 2.2 Calculation of vertices of the $(T_s - T_a) \sim V_c$ trapezoid and its simplification: the $T_s \sim VI$ trapezoid

The theoretical basis of  $(T_s - T_a) \sim V_c$  trapezoid is the energy balance equation, i.e.,

$$R_n = G + H + \lambda E \quad (2)$$

5 where,  $R_n$  is the net radiant heat flux density ( $W m^{-2}$ ),  $G$  is the soil heat flux density ( $W m^{-2}$ ),  $H$  is the sensible heat flux density ( $W m^{-2}$ ), and  $\lambda E$  is the latent heat flux to the air ( $W m^{-2}$ ) and  $\lambda$  the heat of vaporization (kJ/kg).

In their simplest forms,  $H$  and  $\lambda E$  can be expressed as:

$$H = C_v (T_s - T_a) / r_a \quad (3)$$

$$10 \lambda E = [\Delta (R_n - G) + C_v (VPD) / r_a] / [\Delta + \gamma (1 + r_c / r_a)] \quad (4)$$

where

- $T_s$  and  $T_a$  are the land-surface and air temperature (K), respectively;
- $C_v$  is the volumetric heat capacity of air ( $1295.16 J K^{-1} m^{-3}$ );
- VPD (vapor pressure deficit of the air) (hPa) is calculated as a difference between saturation vapour pressure  $e_s$  and actual vapour pressure  $e_a$  (hPa), given by (WMO, 2008)

$$e_s = 6.112 \exp\left(\frac{17.62 T'_a}{T'_a + 243.12}\right) \quad (T'_a \text{ is the air temperature in } ^\circ C, T'_a = T_a - 273.15)$$

$$e_a = \mu e_s, \quad (\mu \text{ is observed relative humidity})$$

8707

- $\Delta$  is the slope of the curve of saturation water vapour pressure versus air temperature, calculated with (WMO, 2008)

$$\Delta = 4098 \cdot e_s / (237.3 + T'_a)^2$$

- $\gamma$  the psychrometric constant (hPa/°C), given by (WMO, 2008)

$$5 \gamma = 0.646 + 0.0006 T'_a$$

- $r_a$  the aerodynamic resistance ( $s m^{-1}$ );
- $r_c$  the canopy resistance to vapor transport ( $s m^{-1}$ );

Then, combining Eqs. (2), (3), and (4), we obtain the equation for temperature difference between air and land surface:

$$10 (T_s - T_a) = [r_a (R_n - G) / C_v] \left\{ \gamma (1 + r_c / r_a) / [\Delta + \gamma (1 + r_c / r_a)] \right\} - VPD / [\Delta + \gamma (1 + r_c / r_a)] \quad (5)$$

As suggested by Moran et al. (1994), for the  $(T_s - T_a) \sim V_c$  trapezoid, its four vertices correspond to (1) well-watered full-cover vegetation, (2) water-stressed full-cover vegetation, (3) saturated bare soil, and (4) dry bare soil. Using the energy balance equations, Moran et al. computed the values of the four vertices of the trapezoid as the following:

(1) For full-covered and well-watered vegetation (Point 1)

$$15 (T_s - T_a)1 = [r_a (R_n - G) / C_v] \left\{ \gamma (1 + r_{cm} / r_a) / [\Delta + \gamma (1 + r_{cm} / r_a)] \right\} - VPD / [\Delta + \gamma (1 + r_{cm} / r_a)] \quad (6)$$

where  $r_{cm}$  is the minimum canopy resistance, i.e., canopy resistance at potential evapotranspiration.

8708

(2) For full-covered vegetation with no available water (Point 2)

$$(T_s - T_a)_2 = [r_a (R_n - G)/C_v] \left\{ \gamma (1 + r_{cx}/r_a) / [\Delta + \gamma (1 + r_{cx}/r_a)] \right\} - \text{VPD} / [\Delta + \gamma (1 + r_{cx}/r_a)] \quad (7)$$

where  $r_{cx}$ , is the canopy resistance associated with nearly complete stomatal closure.

5 (3) For saturated bare soil (Point 3), where canopy resistance ( $r_c$ ) = 0, we have

$$(T_s - T_a)_3 = [r_a (R_n - G)/C_v] [\gamma (\Delta + \gamma)] - \text{VPD} / (\Delta + \gamma) \quad (8)$$

(4) For dry bare soil (Point 4), where  $r_c = \infty$  (analogous to complete stomatal closure), and  $\lambda E = 0$ , we have

$$(T_s - T_a)_4 = r_a (R_n - G)/C_v \quad (9)$$

10 The  $(T_s - T_a) \sim V_c$  trapezoid considers that relationship between  $(T_s - T_a)$  and  $V_c$ . Now we think about the issue in another way that, with a given value of  $T_a$ , how  $T_s$  is related with  $V_c$ . To analysis this  $T_s \sim V_c$  relationship, we use Eq. (6)~(9) to calculate the  $T_s$  for the four extreme cases (or trapezoid vertices) by move  $T_a$  in the equations to the right side of the equations. At the same time,  $V_c$  is replaced by vegetation index (VI). So that, we modify the structure of the trapezoid, obtaining a simplified  $T_s \sim VI$  trapezoid with the horizontal axis as VI, and the vertical axis as the surface temperature  $T_s$ . We therefore refer the algorithm proposed here to as  $T_s - VI$  trapezoid method.

15 To obtain the values of  $T_s$  with Eq. (6)~(9), we need to know  $r_a$ ,  $r_c$  (including  $r_{cm}$  and  $r_{cx}$ ),  $R_n$ ,  $G$  for the four vertices separately, as shown in the following section.

8709

### 2.3 Calculation of the components in the formula for four vertices of $T_s \sim VI$ trapezoid

#### 2.3.1 Aerodynamic resistance ( $r_a$ )

The water vapor aerodynamic resistance  $r_a$  (s/m) can be estimated with the following equation (Brutsaert, 1982):

$$r_a = \left[ \ln \left( \frac{z - d}{z_{0m}} \right) - \psi_m \right] \left[ \ln \left( \frac{z - d}{z_{0h}} \right) - \psi_h \right] / k^2 u_z \quad (10)$$

where

- $z$  is the height (m) above the surface at which  $u_z$  and  $T_a$  are measured (commonly 2 m);
- 10 –  $u_z$  is wind speed ( $\text{m s}^{-1}$ ), which could be measured directly;
- $d$  is displacement height (m), given by  $d = 0.667h$ , and  $h$  is the height of vegetation (Garratt, 1992), which should be given as an input.  
 $z_{0m}$  is the roughness lengths for momentum (m), given by  $z_{0m} = h/8$  (Garratt, 1992). For bare soil surface,  $z_{0m}$  is commonly taken to be 0.01 m (Shuttleworth and Wallace, 1985).
- 15 –  $z_{0h}$  is the roughness lengths for heat (m), given by

$$z_{0h} = z_{0m} / \exp \left( KB^{-1} \right) \quad (11)$$

Here,  $KB^{-1}$  is a dimensionless parameter. Kustas et al. (1989) showed that  $KB^{-1}$  is a linear function of the product of  $u$  and  $T_s - T_a$ , given by

$$20 \quad KB^{-1} = S_{KB} \cdot u \cdot (T_s - T_a) \quad (12)$$

8710

where  $S_{KB}$  is an empirical coefficient, which varies somewhere between 0.05 and 0.25.

–  $k$  is the von Karman constant ( $k = 0.41$ );

–  $\psi_h$  and  $\psi_m$  are the stability corrections for heat and momentum (unitless).  $\psi_h$  and  $\psi_m$  are calculated differently depend on the atmospheric stability, which could be indicated by the Monin-Obukhov length  $L$ , given by

$$L = -\rho C_p u_*^3 T_a / (kgH) \quad (13)$$

where  $g = 9.8 \text{ m/s}^2$ ,  $k = 0.41$ ,  $\rho$  is the air density ( $\text{kg m}^{-3}$ ),  $C_p$  the air specific heat at constant pressure ( $1004 \text{ J kg}^{-1} \text{ K}^{-1}$ ),  $u_* = u_z k / [\ln(z/z_{0m})]$ .

For stable situations ( $L > 0$ ),

$$\begin{cases} \psi_m = -5 (z - z_{0m}) / L \\ \psi_h = -5 (z - z_{0h}) / L \end{cases} \quad (14)$$

For unstable conditions ( $L \leq 0$ ),

$$\begin{cases} \psi_m = 2 \ln \left( \frac{1+x}{1+x_0} \right) + \ln \left( \frac{1+x^2}{1+x_0^2} \right) - 2 \tan^{-1}(x) + 2 \tan^{-1} x_0 \\ \psi_h = 2 \ln \left( \frac{1+y}{1+y_0} \right) \end{cases} \quad (15)$$

where,  $x = [1 - 16(z-d)/L]^{1/4}$ ,  $x_0 = [1 - 16z_{0m}/L]^{1/4}$ ,  $y = [1 - 16(z-d)/L]^{1/2}$ ,  $y_0 = [1 - 16z_{0h}/L]^{1/2}$ .

### 2.3.2 Net radiant heat flux density ( $R_n$ )

Net radiation is defined as the difference between the incoming and outgoing radiation fluxes including both long- and shortwave radiation at the surface of Earth. Net radiant heat flux density ( $R_n$ ) ( $\text{W m}^{-2}$ ) can be expressed as:

$$R_n = (1 - \alpha) R_s + \epsilon_a \times \sigma \times T_a^4 - \epsilon_s \frac{\sigma T_s^4}{8711} \quad (16)$$

where

–  $\alpha$  is surface shortwave albedo, which can be calculated as a combination of MODIS narrow band spectral reflectance values ( $\alpha_1 \sim \alpha_7$ ) (Liang et al., 1999), given by

$$\alpha = 0.3973 \alpha_1 + 0.23821 \alpha_2 + 0.3489 \alpha_3 + 0.265 \alpha_4 + 0.1604 \alpha_5 - 0.0138 \alpha_6 + 0.0682 \alpha_7 + 0.0036$$

–  $R_s$  is solar radiation, estimated jointly by solar constant, solar inclination angle, geographical location and time of year, atmospheric transmissivity, ground elevation, etc. The basic formula for estimating  $R_s$  is (Zillman, 1972):

$$R_s = \frac{S_0 \cos^2 \theta}{1.085 \cos \theta + e_0 (2.7 + \cos \theta) \times 10^{-3} + 0.1}$$

where  $S_0$  is the solar constant at the atmospheric top ( $1367 \text{ W/m}^2$ ),  $\theta$  the solar zenith angle,  $e_0$  is the vapor pressure. In consideration of the effects of topography on the incident short-wave radiation ( $R_s$ ), the solar zenith angle ( $\theta$ ) is corrected using digital elevation model (DEM) data (Duffie and Beckman, 1991) with the following formula:

$$\begin{aligned} \cos \theta &= \sin(\delta) \sin(\varphi) \cos(s) - \sin(\delta) \cos(\varphi) \sin(s) \cos(r) \\ &+ \cos(\delta) \cos(\varphi) \cos(s) \cos(\omega) + \cos(\delta) \sin(\varphi) \sin(s) \cos(r) \cos(\omega) \\ &+ \cos(\delta) \sin(\gamma) \sin(s) \sin(\omega) \end{aligned}$$

where  $\varphi$  is the latitude (positive in the north hemisphere);  $s$  is the slope, and  $r$  is the slope orientation, both derived from DEM;  $\delta$  is solar declination, and  $\omega$  solar hour angle, given by

$$\delta = 0.409 \sin(2\pi \cdot \text{DOY}/365 - 1.39)$$

$$\omega = \frac{\pi}{12} (t - 12)$$

where DOY is the day of year, and  $t$  is the time when the satellite TERRA pass over the region.

–  $\varepsilon_a$  is the atmospheric emissivity estimated as a function of vapor pressure, given by Iziomon et al. (2003)

$$\varepsilon_a = 1 - 0.35 \times \exp(-10 \times e_a/T_a)$$

–  $\varepsilon_s$  is surface emissivity often evaluated as a function of NDVI. For instance,  $\varepsilon_s$  could be predicted for the 8–14  $\mu\text{m}$  spectral range from NDVI using  $\varepsilon_s = 1.009 + 0.047 \ln(\text{EVI})$  (Bastiaanssen et al., 1998). Among MODIS Land Surface Temperature and Emissivity products (MOD11), there are emissivity products for band 31 and 32, i.e.  $\varepsilon_{31}$  and  $\varepsilon_{32}$ . In the present study, we take the average of the two products to get surface emissivity, namely,  $\varepsilon_s = (\varepsilon_{31} + \varepsilon_{32})/2$ .

In our algorithm,  $R_n$  is not directly solved with the Eq. (16), because  $T_s$  is considered as an unknown variable. Instead, we replace the term  $R_n$  in Eq. (6)~(9) with the Eq. (19) respectively, so that we get four quartic equations for  $T_s$  at four vertices separately. Then the quartic equations are solved with the iterative algorithm which is shown later in Sect. 2.4 and Fig. 2, by doing so, all the values of  $T_s$  for the four vertices are obtained.

### 2.3.3 Soil heat flux density $G$

$G$  is normally considered to be linearly related to  $R_n$ . Several studies have shown that the value of  $G/R_n$  typically ranges between 0.4 for bare soil and 0.05 for full vegetation cover (Choudhury et al., 1987). Idso et al. (1975) conducted some experiments investigating the impacts of water content on the net radiation  $\sim$  soil heat flux relationship over bare soil surface, and showed that  $G/R_n$  ranges from 0.2 for wet bare soil to 0.5 for dry bare soil.

8713

### 2.3.4 Canopy resistance ( $r_c$ )

Canopy resistance ( $r_c$ ), including  $r_{cm}$  and  $r_{cx}$  that refer to the minimum and maximum canopy resistance respectively, should be calculated for Point 1 and Point 2. According to Moran et al. (1994),  $r_{cm}$  in Eq. (6) is calculated with  $r_{sm}/\text{LAI}$  (LAI is the leaf area index,  $r_{sm}$  is minimum stomatal resistance).  $r_{cx}$  in Eq. (7) is calculated with  $r_{sx}/\text{LAI}$  ( $r_{sx}$  is maximum stomatal resistance).

Values of minimum and maximum stomatal resistance ( $r_{sm}$  and  $r_{sx}$ , respectively) are published for many agricultural crops under a variety of atmospheric conditions. Moran et al. (1994) suggested that, if values are not available, reasonable values of  $r_{sm} = 25\text{--}100\text{ s/m}$  and  $r_{sx} = 1000\text{--}1500\text{ s/m}$  will not result in appreciable error, we set  $r_{sm} = 25$  and  $r_{sx} = 1500$ . Because LAI are mostly less than 8 (Scurlock et al., 2001), we set  $\text{LAI} = 8$ . Therefore, we have  $r_{cm} = 3.125$  and  $r_{cx} = 187.5$ .

## 2.4 Iterative procedure for calculating $T_s$

Values of  $T_s$  for the four vertices are obtained by an iterative procedure for each pixel. An initial value of  $r_a$  is estimated by ignoring the two stability corrections, i.e.,  $\psi_h$  and  $\psi_m$ . With the initial  $r_a$ , initial values of  $T_s$  are obtained with Eq. (6)~(9) for the four vertices. Then the iterative procedure is proceeded by iteratively changing  $H$ ,  $KB^{-1}$ ,  $r_a$ , and in consequence,  $T_s$ , until the value of  $T_s$  is stable (i.e., the change of  $T_s$  is less than 0.1 K, and the change of  $r_a$  is less than 0.1 s/m). Normally, it takes 5 to 10 iterations. While  $T_s$  is derived,  $R_n$ ,  $G$ ,  $H$ , and  $r_a$  for each vertex are obtained as well.

The iterative procedure is conducted distributedly based on pixels, that is, the trapezoid is constructed separately for each pixel, and each trapezoid has its own values of  $T_s$ .

8714











## 5.2 Calculation of WDI

Based on the constructed  $T_s$ -VI trapezoid for each pixel, using the MODIS  $T_s$  and EVI data, we calculate the WDI for each pixel  $p$ ,

$$\text{WDI}^{(p)} = \frac{T_s^{(p)} - T_{S, \min}^{(p)}}{T_{S, \min}^{(p)} - T_{S, \max}^{(p)}} \quad (20)$$

- 5 where  $T_s$  is surface temperature obtained from MODIS; the subscripts min, max, and r refer to minimum, maximum, and measured values, respectively; and the minimum and maximum values of  $T_s$  are interpolated linearly on the dry edge and wet edge of the  $T_s \sim \text{VI}$  trapezoid for the specific VI value of the pixel.

## 5.3 Comparison with soil moisture observation and precipitation

- 10 Using the surface soil moisture observations at 16 sites, we evaluate WDI estimates in several ways: (1) compared separate WDI estimates with ground observations of all 10 dates (Fig. 8); (2) compare the average of WDI estimates with the average ground observations of 10 dates (Fig. 9); (3) compare the WDI estimates with ground observations of each date separately (Table 2).

- 15 From the scatter plot of WDI vs. observation in Fig. 8, we see that from the perspective of a whole year, WDI estimates derived with the  $T_s$ -VI trapezoid method has a negative correlation (correlation coefficient  $R = -0.7232$ ) with surface soil moisture, which indicates that WDI estimates can be used to detect the temporal variation in soil moisture. Especially on the scale of the watershed, the average WDI is strongly negatively related (correlation coefficient  $R = -0.9$ ) to the average soil moisture observation, as shown in Fig. 9. Although this is not a high correlation, considering that soil moisture in dry environment, such as in semi-arid area, exhibits high spatial variability and potentially rapid rates of temporal change in moisture conditions, the result is reasonably good.

8721

- The comparison between the WDI estimates with ground observations of each date (Table 2) shows that, there is basically no correlation between WDI estimates and surface soil moisture observations. This is partly because of the scale effect, i.e., point soil moisture observations are essentially different from grid averaged soil moisture estimates due to sub-grid variability, partly because of the poor capability of using WDI to detect the variation in soil moisture with low spatial variability. Similar phenomena have been observed by some other researchers as well. For instance, Pellenq et al. (2003) noticed that the point-to-point comparison between observations and simulations shows a poor correlation, but a good correlation is obtained when averaging the simulated and observed soil moisture over a length of 100 m. Comparing the distribution of soil moisture observations over the year with that observed instantaneously, we see that the coefficient of variation (CV) for all soil moisture observations at 16 sites in 10 days over a year is 0.771, much larger than the CV for observed soil in each day (ranging from 0.336 to 0.702, with a mean value of 0.528). In consequence, we can use WDI to detect the temporal variation in soil moisture, but it is hard to detect spatial variation in each day, especially for a small watershed with low spatial soil moisture variability.

- 20 Despite of the poor performance for characterizing the spatial variability of soil moisture with WDI, by a visual inspection of the WDI maps of the WGEW region of the 10 dates in Fig. 10, we can still see a clear spatial pattern of soil moisture distribution, which indicates that, to some extent, soil moisture variability could be depicted by WDI maps.

- 25 We analyzed the impacts of precipitation on soil moisture by calculating the correlation between WDI and antecedent precipitation (AP) of different number of days, and between soil moisture observation and AP of different number of days. The results are illustrated in Fig. 11, which show that WDI and soil moisture observation have similar levels of correlation with AP (one is positive, another is negative), and the maximum correlation occurs when approximately 10-day AP is taken into account. The scatter plot is shown in Fig. 12. The result indicates that, as expected, the temporal variation

8722

of soil moisture (either reflected by ground observations, or by WDI estimates) is significantly dominated by precipitation process.

## 6 Conclusions

5 Considerable efforts have been put on using the relationship between soil moisture and index values derived from surface temperature-vegetation index ( $T_s \sim VI$ ) space, which use optical and thermal RS data as input, to estimate soil moisture. In the present study, we simplified the trapezoidal relationship between the surface temperature and air temperature difference ( $T_s - T_a$ ) vs. the fractional vegetation cover, which is proposed by Moran et al. (1994), to a  $T_s \sim VI$  trapezoid. The trapezoid is constructed separately 10 for each pixel (grid). An iterative algorithm is proposed to estimate the vertices of the  $T_s \sim VI$  trapezoid theoretically. Then water deficit index (WDI) which is calculated based on the  $T_s \sim VI$  trapezoid is calculated for each grid using MODIS remotely sensed measurements of surface temperature and enhanced vegetation index (EVI). In the process of construct the  $T_s \sim VI$  trapezoid, a data pre-processing procedure, including 15 de-stripping bad pixels, eliminating the noise contamination in EVI data, and, especially correcting the topographic effects for air temperature data, is conducted.

Using satellite-based MODIS data (land surface temperature data, EVI, etc.), and ground-based on-site soil moisture data and meteorological data (air temperature, relative humidity, and wind velocity) for the Walnut Gulch Experimental Watershed (WGEW) in Arizona, USA, the capability of using WDI to estimate soil moisture is 20 evaluated using (1) soil moisture observations and (2) antecedent precipitation. The result shows that,  $T_s \sim VI$  trapezoid based WDI can well capture temporal variation in surface soil moisture, but the capability of detecting spatial variation is poor for such a semi-arid region as WGEW.

25 *Acknowledgements.* We are very grateful to USDA Southwest Watershed Research Center for providing observation data of the Walnut Gulch Experimental Watershed. The financial supports from China Postdoctoral Science Foundation (20080431062), the National Science Foundation of China (40771039) and the 111 Project (B08048) are gratefully acknowledged.

8723

## References

- Bastiaanssen, W. G. M. and Menentia, M.: A remote sensing surface energy balance algorithm for land (SEBAL) 1. Formulation, *J. Hydrol.*, 212, 198–212, 1998.
- 5 Bellasio<sup>1</sup>, R., Maffei, G., and Scire, J. S.: Algorithms to Account for Topographic Shading Effects and Surface Temperature Dependence on Terrain Elevation in Diagnostic Meteorological Models, *Bound.-Lay. Meteorol.*, 114, 595–614, 2005.
- Brutsaert, W.: *Evaporation into the Atmosphere: Theory, History and Applications*, D. Reidel, Dordrecht, The Netherlands, 299 pp., 1982.
- Carlson, T. N., Gillies, R. R., and Perry, E. M.: A method to make use of thermal infrared temperature and NDVI measurements to infer surface soil water content and fractional vegetation cover, *Remote Sens. Rev.*, 9, 161–173, 1994.
- 10 Choudhury, B. J., Idso, S. B., and Reginato, J. R.: Analysis of an empirical model for soil heat flux under a growing wheat crop for estimating evaporation by an infrared-temperature based energy balance equation, *Agr. Forest Meteorol.*, 39, 283–297, 1987.
- 15 Duffie, J. A. and Beckman, W. A.: *Solar engineering of thermal process*, 2nd edition, John Wiley and Sons, New York, USA, 1991.
- Garratt, J.: *The Atmospheric Boundary Layer*, Cambridge University Press, New York, USA, 316 pp., 1992.
- 20 Gillies, R. R., Carlson, T. N., Cui, J., Kustas, W. P., and Humes, K. S.: A verification of the “triangle” method for obtaining surface soil water content and energy fluxes from remote measurements of the Normalized Difference Vegetation Index (NDVI) and surface radiant temperature, *Int. J. Remote Sens.*, 18, 3145–3166, 1997.
- Goward, S. N., Cruickshanks, G. D., and Hope, A. S.: Observed relation between thermal emission and reflected spectral radiance of a complex vegetated landscape, *Remote Sens. Environ.*, 18, 137–146, 1985.
- 25 Hassan, Q. K., Bourque, C. P. A., Meng, F. R., and Cox, R. M.: A wetness index using terrain-corrected surface temperature and normalized difference vegetation index derived from standard MODIS products: An evaluation of its use in a humid forest-dominated region of eastern Canada, *Sensors*, 7, 2028–2048, 2007.
- 30 Ian, D. M., Norton, T. W., and Williams, J. E.: Modelling environmental heterogeneity in forested landscapes, *J. Hydrol.*, 150, 717–747, 1993.

- Idso, S. B., Aase, J. K., and Jackson, R. D.: Net radiation – Soil heat flux relations as influenced by soil water content variations, *Bound.-Lay. Meteorol.*, 9, 113–122, 1975.
- Idso, S. B., Jackson, R. D., Pinter Jr., P. J., Reginato, R. J., and Hatfield, J. L.: Normalizing the stress-degree-day parameter for environmental variability, *Agr. Meteorol.*, 24, 45–55, 1981.
- 5 Iziomon, M. G., Mayer, H., and Matzarakis, A.: Downward atmospheric longwave irradiance under clear and cloudy skies: Measurement and parameterization, *J. Atmos. Sol.-Terr. Phy.*, 65, 1107–1116, 2003.
- Jackson, R. D., Idso, S. B., Reginato, R. J., and Pinter, P. J.: Canopy temperature as a crop water stress indicator, *Water Resour. Res.*, 17, 1133–1138, 1981.
- 10 Jennifer, N. H. and McDermid, G. J.: Noise reduction of NDVI time series: An empirical comparison of selected techniques, *Remote Sens. Environ.*, 113, 248–258, 2009.
- Kustas, W. P., Choudhury, B. J., Moran, M. S., Reginato, R. J., Jackson, R. D., Gay, L. W., and Weaver, H. L.: Determination of sensible heat flux over sparse canopy using thermal infrared data, *Agr Forest Meteorol.*, 44, 197–216, 1989.
- 15 Liang, S.: Retrieval of Land Surface Albedo from Satellite Observations: A Simulation Study[J], *J. Appl. Meteorol.*, 38, 712–725, 1999.
- Margulis, S. A., Kim, J., and Hogue, T.: A Comparison of the Triangle Retrieval and Variational Data Assimilation Methods for Surface Turbulent Flux Estimation, *J. Hydrometeorol.*, 6, 1063–1072, 2005.
- 20 McCutchan, M. H. and Fox, D. G.: Effect of Elevation and Aspect on Wind, Temperature and Humidity, *J. Clim. Appl. Meteorol.*, 25(12), 1996–2013, 1986.
- Moran, M. S., Clarke, T. R., Inoue, Y., and Vidal, A.: Estimating crop water deficit using the relation between surface air temperature and spectral vegetation index, *Remote Sens. Environ.*, 49, 246–263, 1994.
- 25 Nemani, R. R. and Running, S. W.: Estimation of regional surface resistance to evapotranspiration from NDVI and thermal IR AVHRR data, *J. Appl. Meteorol.*, 28, 276–284, 1989.
- Nemani, R. R., Pierce, L., Running, S. W., and Goward, S.: Developing satellite-derived estimates of surface moisture status, *J. Appl. Meteorol.*, 32, 548–557, 1993.
- Pellenq, J., Kalma, J., Boulet, G., Saulnier, G. M., Wooldridge, S., Kerr, Y., and Chehbouni, A.:  
30 A disaggregation scheme for soil moisture based on topography and soil depth, *J. Hydrol.*, 276, 112–127, 2003.
- Price, J. C.: Using spatial context in satellite data to infer regional scale evapotranspiration [J], *IEEE T. Geosci. Remote*, 28, 940–948, 1990.

8725

- Renard, K. G., Lane, L. J., Simanton, J. R., Emmerich, W. E., Stone, J. J., Weltz, M. A., Goodrich, D. C., and Yakowitz, D. S.: Agricultural impacts in an arid environment: Walnut Gulch case study, *Hydrol. Sci. Tech.*, 9(1–4), 145–190, 1993.
- 5 Sandholt, I., Rasmussen, K., and Andersen, J.: A Simple Interpretation of the Surface Temperature/Vegetation Index Space for Assessment of Surface Moisture Status, *Remote Sens. Environ.*, 79(2), 213–224, 2002 .
- Scurlock, J. M. O., Asner, G. P., and Gower, S. T.: Global Leaf Area Index Data from Field Measurements, 1932–2000, Data set, available on-line at <http://www.daac.ornl.gov> from the Oak Ridge National Laboratory Distributed Active Archive Center, last access: 1 August 2010, Oak Ridge, Tennessee, USA, 2001.
- 10 Shuttleworth, W. and Wallace, J.: Evaporation from Sparse Crops – An Energy Combination Theory, *Q. J. Roy. Meteor. Soc.*, 111, 839–855, 1985.
- Skirvin, S., Kidwell, M., Biedenbender, S., Henley, J. P., King, D., Collins, C. H., Moran, S., and Weltz, M.: Vegetation data, Walnut Gulch Experimental Watershed, Arizona, United States, *Water Resour. Res.*, 44, W05S08, doi:10.1029/2006WR005724, 2008.
- 15 Smith, R. C. G. and Choudhury, B. J.: Analysis of normalized difference and surface temperature observations over southeastern Australia, *Int. J. Remote Sens.*, 12(10), 2021–2044, 1991.
- Tang, R., Li, Z.-L., and Tang, B.: An application of the  $T_sVI$  triangle method with enhanced edges determination for evapotranspiration estimation from MODIS data in arid and semi-arid regions: Implementation and validation, *Remote Sens. Environ.*, 114, 540–551, 2010.
- Velleman, P.: Definition and comparison of robust nonlinear data smoothing algorithms, *J. Am. Stat. Assoc.*, 75, 609–615, 1980.
- World Meteorological Organization (WMO): Guide to Meteorological Instruments and Methods of Observation, WMO-No. 8 (CIMO Guide), Geneva, 2008.
- 25 Zillman, J. W.: A study of some aspects of the radiation and heat budgets of the southern hemisphere oceans, Canberra: Australian Government Publishing Service, Canberra, Australia, 1972.

8726

**Table 1.** MODIS data used in the present study.

Product ID	Contents	Spatial resolution	Temporal resolution
MO03	Geolocation Data Set	1 km	daily
MOD09A1	Surface Reflectance	500 m	8 days
MOD11A1	Surface Temperature and Emissivity	1 km	daily
MCD12Q1	Land Cover and Vegetation Dynamics	500 m	Yearly
MOD13A1	Vegetation Indices	250 m	8 days
MOD15A2	Leaf Area Index	1 km	8 days

8727

**Table 2.** Correlation coefficients between WDI estimates with surface soil moisture observations.

DOY	345	290	256	212	168	157	132	75	30	2
<i>R</i>	0.1225	-0.0316	0.0632	0.0775	-0.0447	-0.0775	-0.2049	0.2098	-0.4919	0.0548

8728

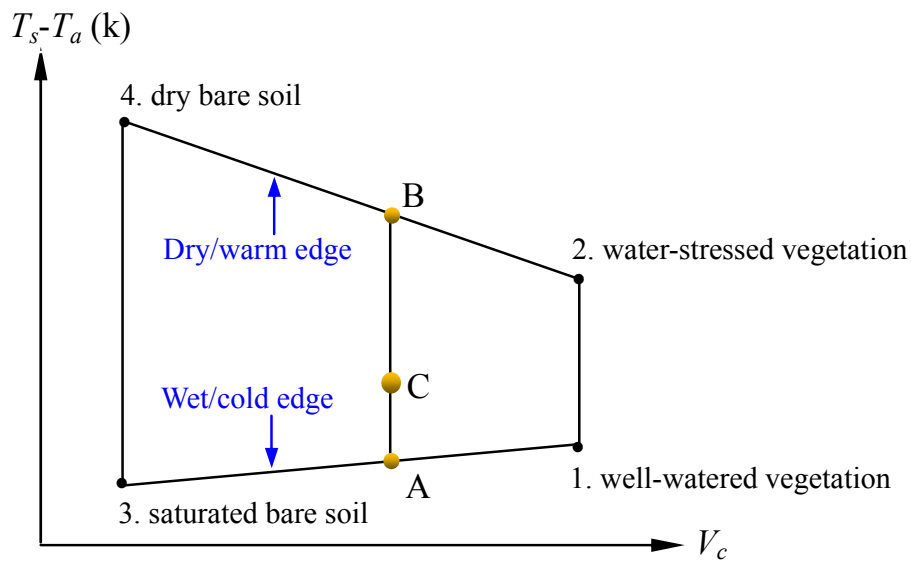


**Fig. 1.** The hypothetical trapezoidal shape based on the relation between  $(T_s - T_a)$  and the fractional vegetation cover ( $V_c$ ).

8729

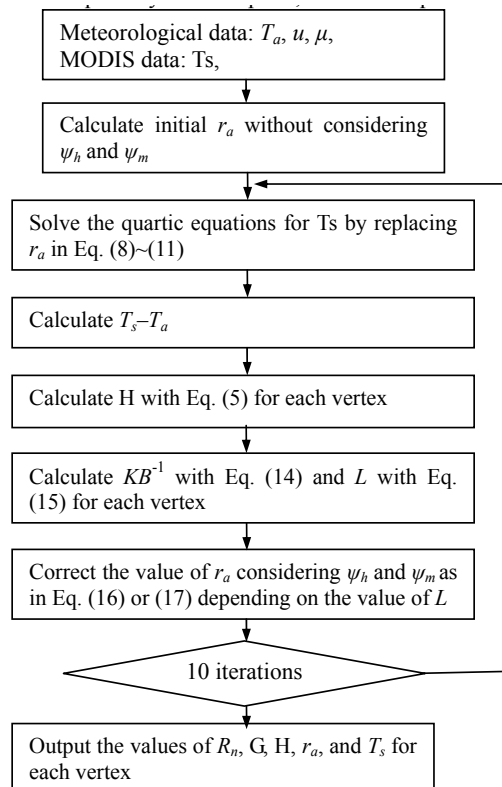


**Fig. 2.** Iterative procedure for calculating  $T_s$  of the four vertices of  $T_s$ -VI trapezoid.

8730



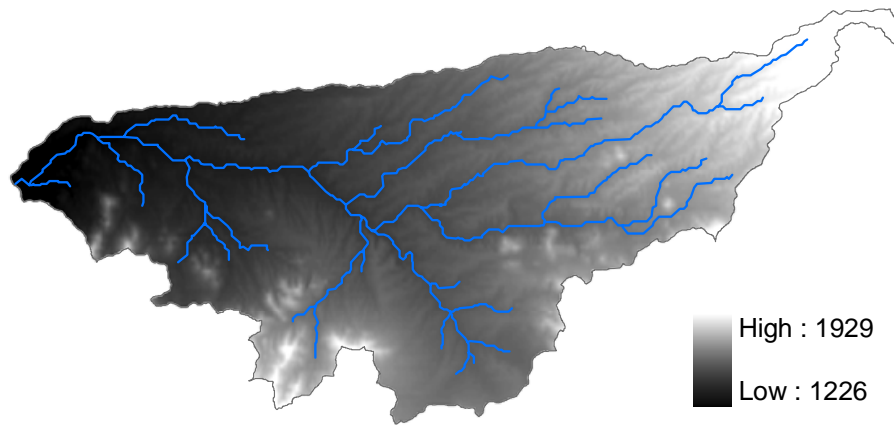


Fig. 3. Digital elevation model (DEM) of Walnut Gulch Experimental.

8731

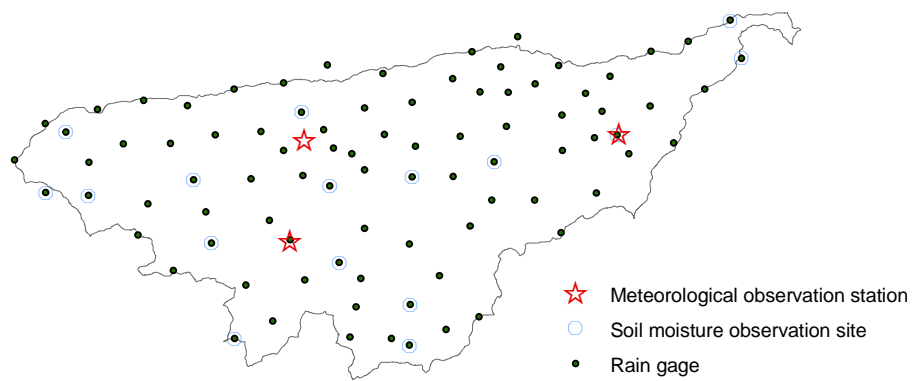
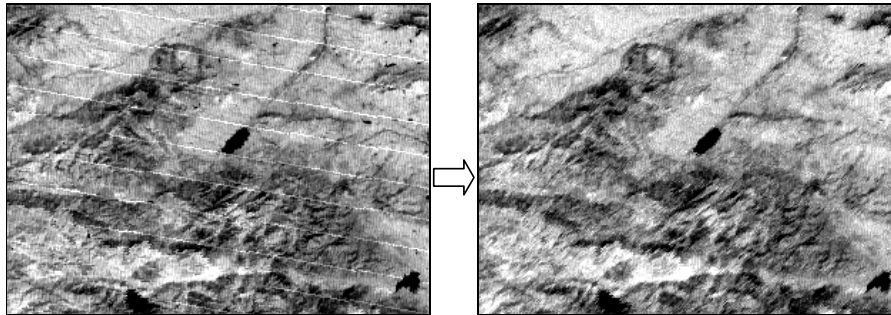


Fig. 4. Locations of ground-based observation sites in WGEW.

8732



**Fig. 5.** Comparison of Band 5 albedo images before (left) and after destriping.

8733

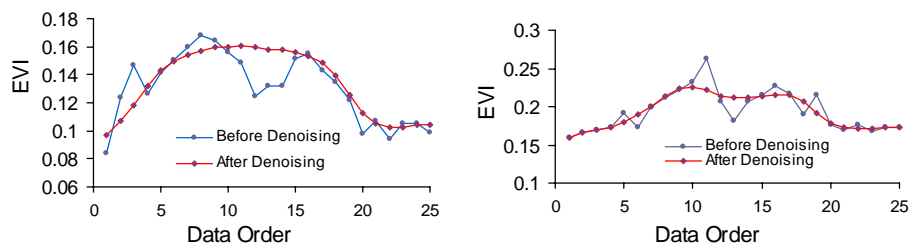


**Fig. 6.** Effects of EVI denoising preprocessing for two randomly selected pixels.

8734

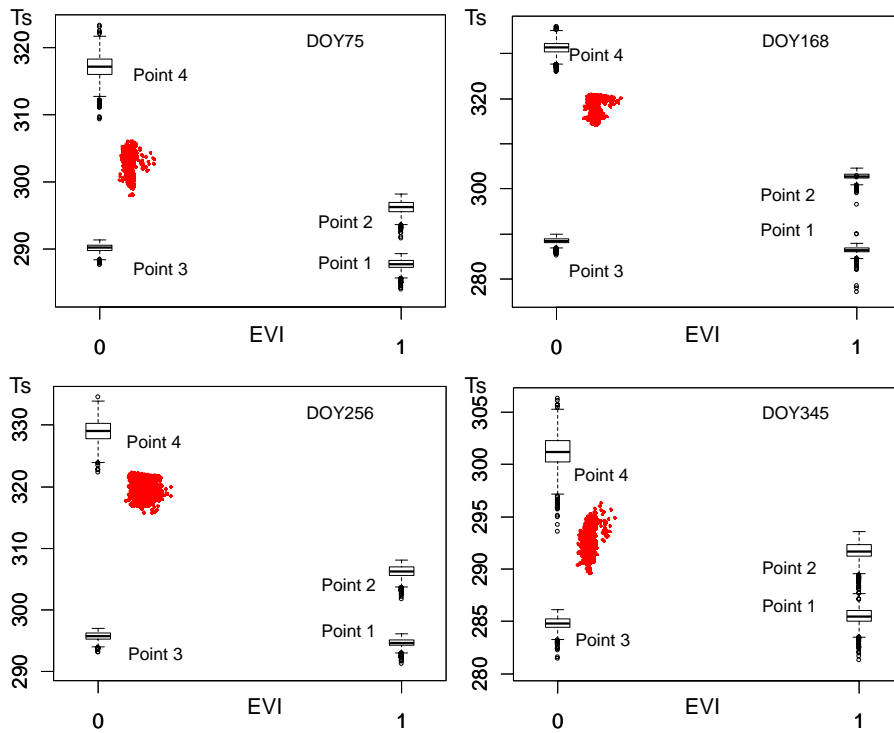


**Fig. 7.** Constructed  $T_s$ -EVI trapezoids in four dates in four different seasons.

8735

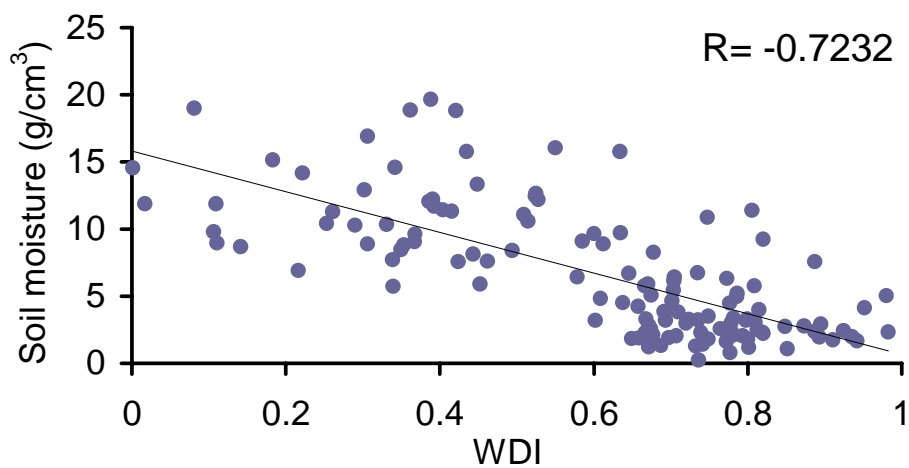


**Fig. 8.** WDI estimates vs. ground observations at 16 sites in 10 dates ( $R$  is the correlation coefficient).

8736

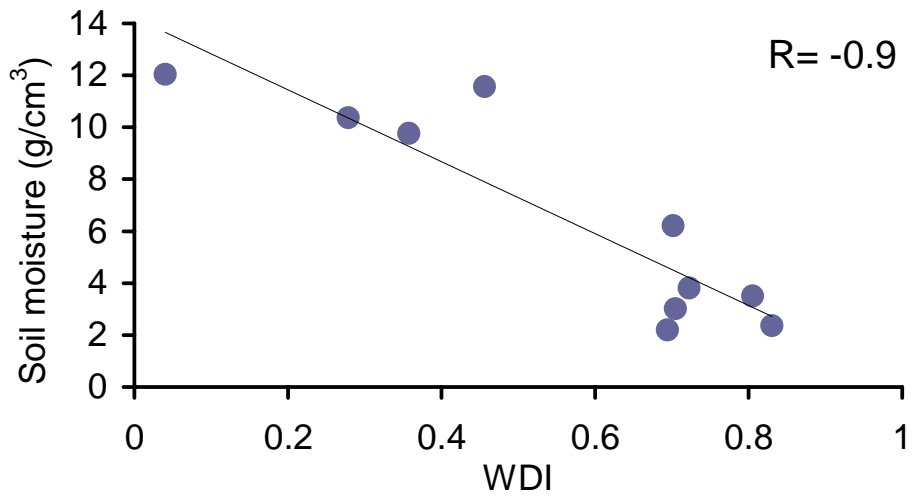


**Fig. 9.** The average WDI estimates vs. the average ground observations in 10 dates ( $R$  is the correlation coefficient).

8737

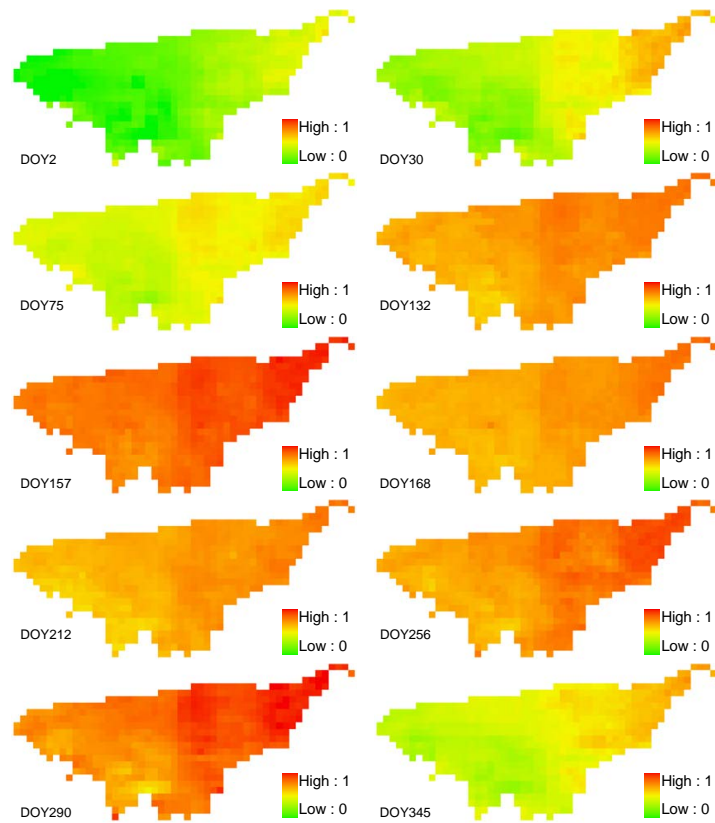


**Fig. 10.** WDI maps for 10 DOYs.

8738

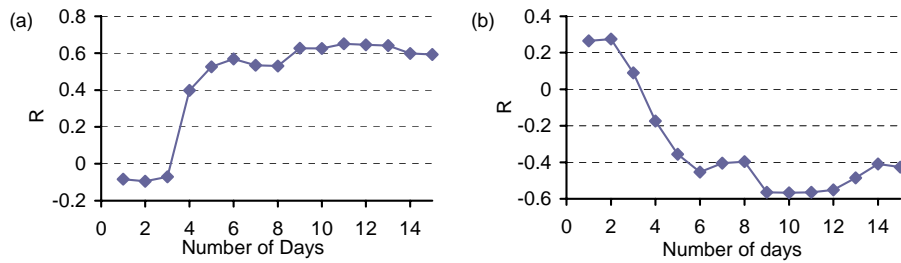


**Fig. 11.** Correlation coefficient ( $R$ ) between (a) soil moisture observation and AP of different number of days, and (b) WDI and AP of different number of days.

8739

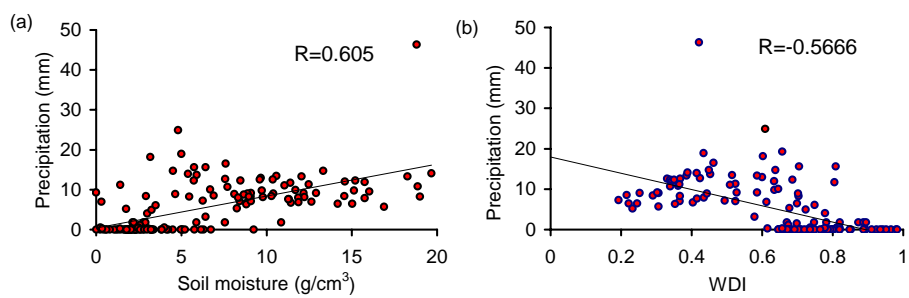


**Fig. 12.** Scatter plot of (a) soil moisture observation and (b) WDI vs. 10-day AP ( $R$  is the coefficient of correlation).

8740